Properties of nanoporous silica thin films determined by high-resolution x-ray reflectivity and small-angle neutron scattering

Wen-li Wu, William E. Wallace,[a] Eric K. Lin, and Gary W. Lynn[b]
Polymers Division, National Institute of Standards and Technology, 100 Bureau Drive, Gaithersburg, Maryland 20899-8541

Charles J. Glinka
Center for Neutron Research, National Institute of Standards and Technology, 100 Bureau Drive, Gaithersburg, Maryland 20899-8562

E. Todd Ryan and Huei-Min Ho
SEMATECH, 2706 Montopolis Drive, Austin, Texas 78741-6499

(Received 20 May 1999; accepted for publication 18 October 1999)

A new methodology based on a novel combination of a high-resolution specular x-ray reflectivity and small-angle neutron scattering has been developed to evaluate the structural properties of low-dielectric-constant porous silica thin films about one micrometer thick supported on silicon wafer substrates. To complement these results, film composition was determined by high-energy ion scattering techniques. For the example thin film presented here, the overall film density was found to be (0.55 ± 0.01) g/cm^3 with a pore wall density of (1.16 ± 0.05) g/cm^3 and a porosity of (53 ± 1)%. The characteristic average dimension for the pores was found to be (65 ± 1) Å. It was determined that (22.1 ± 0.5)% of the pores had connective paths to the free surface. The mass fraction of water absorption was (3.0 ± 0.5)% and the coefficient of thermal expansion was $(60\pm20)\times10^{-6}$/°C from room temperature to 175 °C. Lastly, model fitting of the specular x-ray reflectivity data indicated the presence of a thin surface layer with an increased electron density compared to the bulk of the film as well as an interfacial layer with a reduced electron density. [S0021-8979(00)00703-9]

I. INTRODUCTION

In modern integrated circuitry multilevel interconnection is typically used to create logic devices from individual transistors. By employing the third dimension, interconnect distances can be greatly reduced; furthermore, silicon wafer area is preserved for active devices and not for passive conductors.[1] For the materials used to create these interlevel dielectric layers, stringent material requirements demand an exacting combination of electrical, thermal, chemical, and structural properties which must be met at submicron dimensions and be uniform over the full area on wafers up to 300 mm in diameter. Porous silica films are leading candidates for next-generation low-dielectric-constant thin films to be used as interlayer dielectric materials.[2] The introduction of voids in the material can effectively lower the dielectric constant of the base material. For example, when the film porosity approaches three-quarters by volume, the dielectric constant of silica, nominally about 4, can be reduced to about 2.[3] This lowered dielectric constant has the effect of increasing signal propagation speed, decreasing the energy needed to propagate a signal, and decreasing the crosstalk between adjacent conductors. Many techniques have been established to characterize the performance properties for interlevel dielectric thin films.[4] However, there are few means to measure structural properties, such as porosity and pore size, of porous films less than 1 μm thick, positron annihilation lifetime spectroscopy being one of the few examples.[5–7] Since these structural properties are intimately related to the performance properties, the lack of suitable measurement techniques has prevented the more rapid development of porous interlevel dielectrics.

The purpose of this work is to develop a methodology to characterize porous thin films about 1 μm thick supported on silicon wafers. The characterization must be done while the films remain adhered to the silicon substrate because the porous films are generally too fragile for removal from the substrate. Furthermore, the porous structure prepared on the substrate may be altered by processing off wafer, that is, in bulk state. The structural properties to be measured include overall film density, pore-wall density, porosity, average pore size, and pore connectivity. The first four parameters are important for correlating observed thermomechanical behavior with structure so that improvements in material selection and/or material processing can be accelerated. The last parameter is important in cases where the films are exposed to wet environments such as in chemical-mechanical polishing processes. A connected pore structure may result in an uncontrolled increase in the dielectric constant or leakage current due to the penetration of any contaminant materials, but there is little published data to confirm this. In addition to these structural properties, the out-of-plane coefficient of thermal expansion (CTE) and the electron density profile depth normal to the sample surface were also measured.

[a]Electronic mail: william.wallace@nist.gov
[b]Also at Department of Chemistry, University of Tennessee, Knoxville.

The key measurement techniques used in this work are specular x-ray reflectivity (SXR)[8–10] and small-angle neutron scattering (SANS).[11] The fundamentals of these two techniques are widely discussed in the literature and will only be briefly described here. The novelty of the present work is twofold: the use of a new high-resolution x-ray reflectometer to accurately measure the thickness of films about 1 μm thick, and the treatment of complementary data obtained from both SXR and SANS as a set of simultaneous equations to quantitatively determine the structural parameters of the porous thin films. A 900-nm-thick porous silica (xerogel) thin film test sample, AlliedSignal Nanoglass™ K2.2-A10B, is characterized using these techniques to demonstrate the utility of this methodology.[12] The films used were prepared by spin coating using sol-gel methods.[13,14]

In this work, we used the simplest description of a porous material; a two-phase model where one phase comprises the voids and the other comprises the connecting material. The material between the voids (the pore wall material) is assumed to be uniform in density. This assumption results in two unknowns, the porosity, P, and the wall density, ρ_w. These two variables cannot be separated from either SXR or SANS data alone. Therefore, we performed both measurements on the same sample. By solving simultaneous equations, specific to each technique, involving the two variables the values of the unknowns can be determined. In order to perform this separation, we must also know the chemical composition of the thin film. These compositions were determined using a combination of Rutherford backscattering (RBS) (for silicon, oxygen, and carbon) and forward recoil elastic scattering (FRES) (for hydrogen). The film composition is used to convert the electron density to mass density in SXR data analysis, and to determine the scattering contrast between the connecting material and pores in the SANS work.

The questions of pore connectivity and moisture uptake were addressed by conducting SANS measurements on a sample immersed respectively in either a deuterated organic solvent or in deuterated water. Solvents with low interfacial tension can readily fill interconnected pores having a passage to the exterior surface. Deuterated toluene is such a solvent and spreads readily on the surfaces of all samples tested to date with a contact angle of generally less than 5°. On the other hand water was found to have a much higher contact angle, typically near 90°, and consequently was found not to fill the pores of the sample. Once the pores are filled, the scattering contrast changed dramatically depending on the neutron scattering length of the solvent used. The percentage of the pores filled by solvent or water is estimated from the difference in SANS intensity between thin films before and after immersion.

The coefficient of thermal expansion normal to the sample surface is performed using film thickness information from the spacing of the interference fringes in the SXR data as a function of temperature. The electron density profile normal to the sample surface is found by modeling the SXR data and provides important insights into the film structure. The films were not uniform in electron density with deviations at the free surface and at the interface with the silicon substrate.

II. EXPERIMENTAL PROCEDURES

A. X-ray reflectivity

At an x-ray wavelength of a few tenths of a nanometer, the refractive index of most materials is less than one.[8] Hence, there exists a critical angle below which total external reflection of the radiation takes place. This critical angle, θ_c, can be approximated by $(\rho r_e \lambda^2/\pi)^{0.5}$ where ρ is the electron density or the number of electrons per unit volume of the material, λ is the x-ray wavelength, and $r_e = 2.818$ fm is the classical electron radius. All the angles used within the context of x-ray reflectivity are defined as grazing angles measured from the surface parallel. At any incident angle below θ_c total reflection occurs. In a typical SXR measurement, the reflected intensity is collected as a function of the incident angle as it is continuously varied through the critical angle. By modeling the SXR result with a one-dimensional Schrödinger equation, the details of the electron density depth profile can be deduced.[15] Free-surface roughness, interfacial roughness, and density variations in the thickness direction can also be determined using computer modeling to create electron-density depth profiles that best fit the experimental data. The information reported here from SXR is an average over a lateral dimension of a few micrometers as dictated by the coherence length of the x-ray beam.

The SXR results are specular data collected with the grazing incident angle equal to the detector angle. The angle ranged from 0.05° to 0.6°. The SXR measurements were conducted in a θ–2θ configuration with a fine focus copper x-ray tube. The incident beam was conditioned with a four-bounce germanium [220] monochromator. Before the detector, the beam was further conditioned with a three-bounce germanium [220] channel cut crystal. This configuration results in a copper $K_{\alpha 1}$ beam with a fractional wavelength spread, $\Delta\lambda/\lambda$, of 1.3×10^{-4} and an angular divergence of 12 arcsec. The motion of the goniometer is controlled by a closed-loop active servo system with an angular reproducibility of 0.0001°. These high precision settings in both the x-ray optics and the goniometer control are necessary to detect the very narrowly spaced interference fringes from films on the order of 1 μm thick.

B. Small angle neutron scattering

The small angle neutron scattering measurements were conducted on the NG1 instrument at the Center for Neutron Research at the National Institute of Standards and Technology. Small angle neutron scattering was performed on thin film samples in a straightforward fashion with the beam incident along the surface normal. The wavelength, λ, was 6 Å with a wavelength spread, $\Delta\lambda/\lambda$, of 0.25. The sample to detector distance was 3.6 m. The detector was offset by 3.5° from the incident beam to increase the observed angular range. The resultant scattering vector, q [where $q = (4\pi/\lambda)\sin(\theta/2)$ and θ is the scattering angle from the incident beam path] ranged from 0.01 to 0.18 Å^{-1}. The SANS results and the structural parameters deduced from them are

quantities averaged over the scattering volume of approximately 1 $cm^2 \times 5\,\mu m$. To enhance the scattering signal, the SANS samples were composed of a stack of six or more pieces of the wafer with the thin film attached. This is a well-documented technique for the study of thin films on silicon substrates by SANS.[16] Rectangular quartz cells were used to hold the samples. Since the silicon wafer substrate supporting the porous film is transparent to neutrons and the wafer does not cause any scattering in the angular range of interest, the scattered intensities in the small angle region (less than 5°) are exclusively from the porous film. This assumption was tested by measuring the scattering from a stack of six bare silicon wafers. The silicon wafers themselves produced almost no small angle scattering. Two-dimensional scattering intensity data were collected from each thin film sample stack and were corrected for the empty quartz cell scattering, background counts, detector uniformity, and sample thickness. The scattering intensity data were reduced to an absolute scale by using a 1.0-mm-thick water sample as a standard. The two-dimensional data were circularly averaged to produce one-dimensional intensity profiles. The scattering contrast arises from the difference in the neutron scattering length of the connecting pore wall material and the pores themselves (taken to be zero).

For the thin film sample studied, three different SANS samples were prepared; one in air, one with the sample immersed in deuterated toluene (*d*-toluene), and one with the sample in deuterated water. The samples were immersed in both solvents for at least 24 h before measurement. The SANS results from the air samples are used in conjunction with the SXR results to determine wall material density, ρ_w, porosity, P, and the size of the pores, as previously discussed. The SANS results from *d*-toluene-immersed samples were analyzed to determine the pore connectivity. The deuterated water sample results were used to determine moisture uptake.

C. High-energy ion scattering measurements

The chemical composition of the porous silica films was determined by high-energy ion scattering techniques.[17] The ion scattering reported here was performed at the Surface and Thin Film Analysis Facility at the University of Pennsylvania, Philadelphia. A well collimated, monoenergetic beam of α particles is directed toward the thin film sample held in vacuum. The scattered energy of the α particles is proportional to the mass of each target species, in this case silicon, oxygen, and carbon atoms in the thin film. By detecting the relative number of scattered α particles as a function of energy, and applying the known scattering cross-section for each element, direct integration or computer modeling of the scattering peaks gives the relative abundance of each element. This technique is generally termed Rutherford backscattering spectrometry (RBS). Hydrogen, being lighter than the α particles used, does not show a backscattering signal. Instead it is forward recoiled upon impact with an incoming α particle. By directing the particle beam at grazing incidence to the sample surface (here 15° was used), hydrogen atoms in the sample can be forward recoiled to a detector. Composition analysis is performed in the same manner as with RBS. This technique is termed forward recoil elastic scattering (FRES) or elastic recoil detection (ERD).

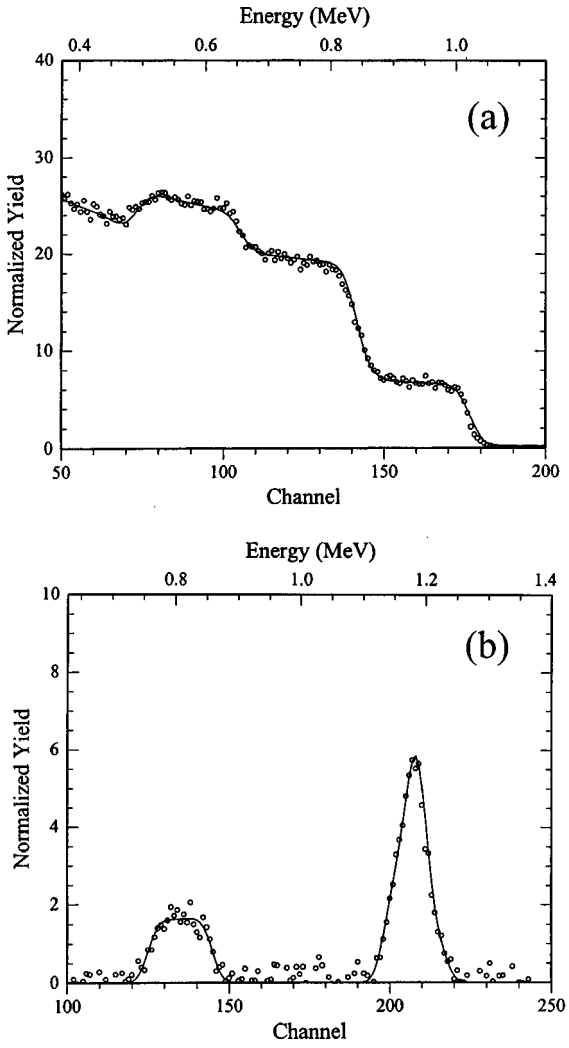

FIG. 1. (a) Rutherford backscattering spectrum for a Nanoglass™ thin film using 1.8 MeV α particles as a probe and the beam incident on the sample at a grazing angle of 15°. (b) Rutherford backscattering spectrum of the same sample using 3.4 MeV α particles as a probe and the beam incident normal to the sample surface. The abscissa gives the energy of the backscattered particle and the ordinate the number of particles of a given energy. The solid line is a simulation of the scattering process for a film of a given composition and thickness. From this simulation the relative amounts of silicon, oxygen, and carbon in the film are determined. See text for feature identification.

III. RESULTS AND DISCUSSION

A. Film composition

The data in Fig. 1 shows a typical RBS spectrum for a Nanoglass™ thin film. The top panel is taken with the beam at a grazing incidence of 15° from the sample surface and at an α-particle beam energy of 1.8 MeV. The plateau from channels 140 to 180 arises from the silicon atoms in the porous silica thin film. The large, high plateau from channels 50 to 140 is from the silicon in the water substrate. Oxygen is represented by the peak at channels 70 to 110. The bottom panel is taken with the beam at normal incidence to the

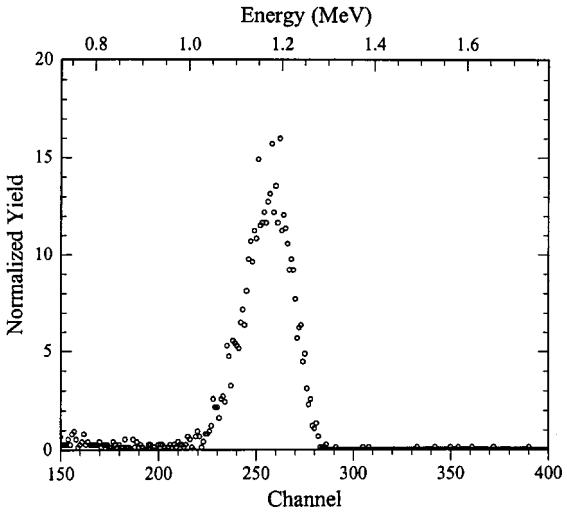

FIG. 2. Forward recoil elastic scattering spectrum for the same Nanoglass™ thin film as shown in Fig. 1. In this case, the 3.0 MeV α particles, incident at grazing angle, expel a small number of the hydrogen atoms from the film at high energy. Their amount in the sample can be found by direct integration of the peak. This data combined with an RBS spectrum like the one in Fig. 1 gives the complete film composition.

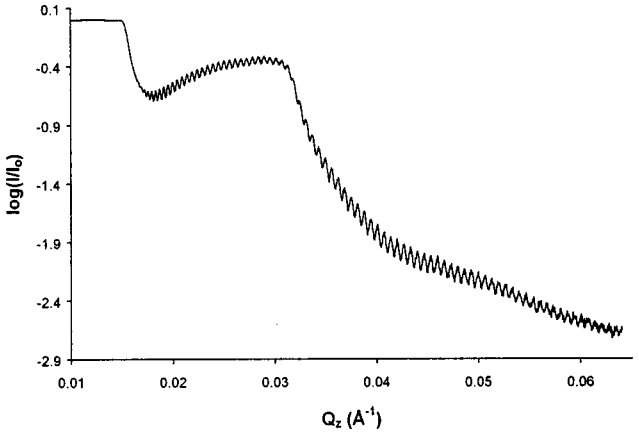

FIG. 3. Specular x-ray reflectivity curve showing the log of the reflectivity vs the momentum transfer normal to the sample surface, Q_z, for an approximately one micrometer thick Nanoglass™ thin film deposited on a silicon wafer. The steep drop in the curve at $Q_z = 0.155\ \text{Å}^{-1}$ is the critical edge for reflection for the porous silica thin film. This value reflects the average electron density of the film. The steep drop at $Q_z = 0.032\ \text{Å}^{-1}$ is the critical edge of the silicon substrate and is determined by the electron density of silicon. The oscillations between the two critical edges are the wave guide modes for x rays confined in the film (analogous to an optical fiber). The oscillations at values of Q_z greater than the silicon critical edge are due to constructive and destructive interference between x rays reflected from the air/film surface and x rays reflected from the film/substrate interface. These oscillations provide a very sensitive measure of film thickness.

sample surface and at a beam energy of 3.4 MeV. The silicon background from the substrate substrated out using a spline fit. The peak from channels 190 to 220 represents oxygen and the peak from channels 120 to 150 represents carbon. The solid line in each panel is a simulation to the data from which the film composition was derived. Often it is easier to simulate the data for a complex multielement film than it is to attempt to integrate peaks exclusive of the background upon which they rest. Figure 2 shows a typical FRES spectrum from a silica thin film. Since only a single element (hydrogen) is measured, only a single scattering peak is seen. In the FRES case direct peak integration was easily performed. By combining both the RBS and FRES results, the composition of this sample was determined to be 19 silicon atoms, 34 oxygen atoms, 14 carbon atoms, and 33 hydrogen atoms per 100 atoms total with an estimated standard uncertainty of ± 5 atoms for each element. (Uncertainties represent standard deviations of the data). The detection limit is on the order of 5% for each element as well.

B. Overall film density

SXR results are typically presented as the logarithm of the ratio of the reflected beam intensity (I) to the incident beam intensity (I_0) versus Q_z, as shown in Fig. 3. Q_z is the magnitude of x-ray momentum transfer in the film thickness direction and is defined as $(4\pi/\lambda)\sin\theta$, where λ is the copper $K_{\alpha 1}$ wavelength of 0.154 06 nm and θ is the grazing incident angle. The SXR data show two critical angles, one at $Q_z = (0.0155 \pm 0.0003)\ \text{Å}^{-1}$ and the other at $Q_z = (0.0320 \pm 0.0006)\ \text{Å}^{-1}$. The critical angle at $Q_z = 0.0155\ \text{Å}^{-1}$ is attributed to the thin film and its position can be related to the thin film electron density. The critical angle at $Q_z = 0.0320\ \text{Å}^{-1}$ corresponds to that of the silicon wafer. The electron density of the thin film calculated from the critical Q_z is $1.693 \times 10^{23}\ \text{e}^-/\text{cm}^3$. Given the chemical composition of the films from the ion scattering measurements, the mass density of the film is calculated to be $(0.55 \pm 0.01)\ \text{g/cm}^3$.

Without independent information about the wall density and porosity, the porosity of the film must be determined from the SXR data with estimates of the wall material density. If one assumes that the density of the material between the pores is that of a typical thermal oxide, 2.25 g/cm^3, then the corresponding porosity will be 75.6% by volume. If one assumes that the density of the material between the pores is that of a typical hydrogen silsesquioxane (HSQ) spin-on glass material, 2.00 g/cm^3, then the corresponding porosity will be 72.6% by volume. Since the composition of this thin film is not just silica but contains a significant fraction of hydrocarbons, the density of the material between the pores is expected to be different from that of either thermal oxide or a typical HSQ. In addition, the density of HSQ-type materials depends strongly on processing conditions.[18]

The validity of the above wall density assumptions can be tested by using a complementary experimental technique. The mass density of the thin film as a whole is simply a product of the connecting material density between the pores, ρ_w, and the volume fraction occupied by the material, $1-P$. From the SXR and composition data, we have thus far determined only the average film mass density. The remaining objective is to apply a second independent technique to obtain another measurable quantity also related to both ρ_w and P. With two measurements containing ρ_w and P in different forms, one can solve the simultaneous equations and deduce the value of ρ_w and P experimentally. SANS is the technique we chose to fulfill this need. In addition, SANS results provide information related to the size of the pores.

C. Pore wall density and pore structure

Since the thin films are composed of nanopores with a high volume content, a suitable model to describe such a structure uses a density correlation function developed for a random two-phase structure by Debye *et al.*;[19] $\gamma(r)=\exp(-r/\xi)$ where ξ is the correlation length. The average dimension, or the chord length, of the pores is $\xi/(1-P)$, and the average dimension of the wall between the pores is ξ/P. The SANS intensity based on this model takes the form of

$$I(q)=\frac{8\pi P(1-P)\Delta\rho_n^2\xi^3}{(1+q^2\xi^2)^2}, \tag{1}$$

where $\Delta\rho_n$ is the neutron scattering length contrast between two phases. For the present case, this value is the neutron scattering length of the connecting material between the pores since the scattering length of the pores themselves is zero. The neutron scattering length, and hence $\Delta\rho_n$, is linearly proportional to the atom or mass density, an important material parameter to be determined. Explicitly, $\Delta\rho_n$ equals ρ_{wn}, the neutron scattering length of the material between pores. In turn, ρ_{wn} equals $(\Sigma n_i b_i/\Sigma n_i m_i)\rho_w$ where n_i is the atomic fraction of element i, b_i is the neutron scattering length of element i, m_i is the atomic weight of that element, and ρ_w the mass density of the connecting material between pores. Given this relationship and the chemical composition from ion scattering measurements, only ρ_w, a parameter of interest, is unknown. To extract data from the SANS experiment, we first rearrange Eq. (1) as

$$\frac{1}{I(q)^{1/2}}=\frac{1}{(c\xi^3)^{1/2}}+\frac{\xi^2q^2}{(c\xi^3)^{1/2}}, \tag{2}$$

where c is defined as $8\pi P(1-P)\Delta\rho_n^2$. Two quantities, c and ξ, from Eq. (2) can be determined from the slope and the zero q intercept of the SANS data plotted as $I(q)^{-1/2}$ vs q^2. The quantity c is related to the porosity, P, and the mass density of the wall material, ρ_w as $P(1-P)\rho_w^2$. In the previous section on SXR, the thin film density is given by $\rho_w(1-P)$ and has already been measured. Using Eq. (1) from SANS and the relation, $\rho_w(1-P)$, from SXR, one can solve for P and ρ_w.

SANS data are given in Fig. 4 as $I(q)^{-1/2}$ vs q^2. Equation (2) seems to be a valid expression for the scattering intensities except in the low q region. This observation holds true for all samples tested so far and suggests that the Debye model [given by Eq. (1)] is valid for describing the porous materials in this study. A strong scattering intensity in the low q region, often referred to as ''strong forward scattering,'' is typically observed in gels including silica gels, crosslinked polymers, and porous materials such as shale. The origin of this observed strong forward scattering is believed to be associated with the nonuniform distribution of the pores, or with larger length scale heterogeneities, e.g., clustering of pores. Details of this aspect of the data interpretation are not resolved and will not be addressed in this report. The slope and the $q=0$ intercept of Fig. 4 are determined to be $(163.2\pm0.9)\ \mathrm{cm}^{1/2}\,\text{Å}^2$ and $(0.175\pm0.002)\ \mathrm{cm}^{1/2}$, respectively. Given that the mass density of this sample is $(0.55\pm0.01)\ \mathrm{g/cm}^3$, as determined from SXR and ion scattering, the SANS results leads to a porosity of $(53\pm1)\%$, a density of the wall material, ρ_w, of $(1.16\pm0.05)\ \mathrm{g/cm}^3$, and a pore chord length of (65 ± 1) Å.

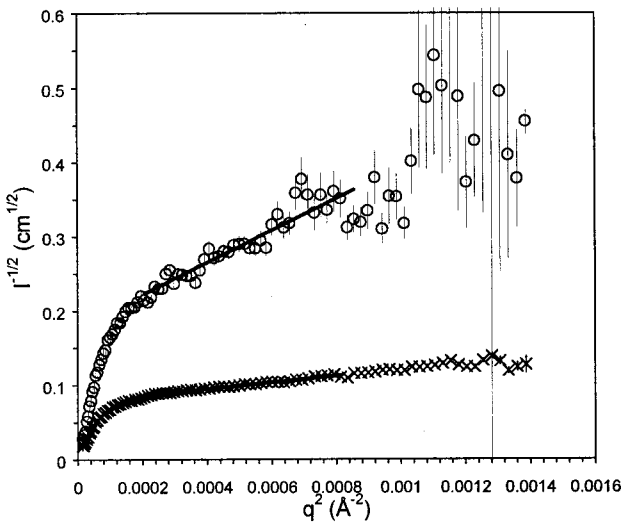

FIG. 4. Debye plot derived from a small angle neutron scattering experiment on a stack of Nanoglass™ thin films (with the silicon substrate attached). The open circles are for the films as-received and the crosses are for the films immersed in deuterated toluene. The uncertainty at each point is proportional to the square root of the number of counts. The slope of the fitted line provides the correlation length of the porous structure. The intercept of the fitted line at $q^2=0$ gives a measure of the porosity and the mass density of the pore wall material.

D. Pore interconnectivity

To determine the fraction of the pores that are interconnected and have a passage to the exterior surface, SANS measurements were also carried out with the same sample immersed in *d*-toluene, a solvent that completely wets the thin film. If all pores are filled with *d*-toluene, the SANS intensity is easily related to that of the sample in air. The SANS contrast factor $\Delta\rho_n$ of Eq. (1) would be replaced by the difference between the pore wall material and the *d*-toluene. The relatively high neutron cross section of *d*-toluene significantly enhances the contrast over that between the pore wall material and air. Given the ρ_n for *d*-toluene, the contrast factor, $\Delta\rho_n^2$, is enhanced by a factor of 18.3. Consequently, the SANS intensity over the entire q region is expected to uniformly increase by the same factor. However, the SANS data from the samples immersed in *d*-toluene have a qualitatively different shape, as seen in Fig. 4, as well as an increase in intensity less than a factor of 18.3. This provides evidence that the pores are not fully filled with solvent during immersion. In addition, the correlation length deduced from the SANS data obtained from *d*-toluene immersed samples was different from that of the dry ones. This suggests that only a selected population of the pores is filled by *d*-toluene. In order to estimate the fraction of pores filled with *d*-toluene, the following two-layer model is introduced: the film immersed in *d*-toluene is made of a wetted layer within which all the pores are filled, and a dry layer. An alternative model for a partially filled system is a random model in which all the filled and unfilled pores are

intermixed and distributed randomly. This random model is less realistic because an empty pore adjacent to a filled pore has a greater probability of also be filled; therefore, this model was not used. Based on the two-layer model for solvent distribution in the film, the SANS intensity at $q=0$ is simply

$$I_t(q=0)=\Phi(\rho_{wn}-\rho_t)^2P(1-P)+(1-\Phi)\rho_{wn}^2P(1-P), \tag{3}$$

where Φ is the volume fraction of the thin film occupied by the toluene-wetted layer, and ρ_t is the neutron scattering density of *d*-toluene. Among the quantities appearing in the above equation, $I_t(q=0)$, the measured SANS intensity of the *d*-toluene immersed sample at zero *q*, the porosity *P*, and the neutron scattering length of the connecting material ρ_{wn} are calculated as described earlier, while the *d*-toluene neutron scattering length, ρ_t, is available from literature. The value of Φ, the volume fraction of pores filled by *d*-toluene, was determined to be $(22.1\pm0.05)\%$ and represents those pores that are interconnected with access to the exterior surface.

E. Moisture uptake

To estimate the moisture uptake of the thin film, a new sample was immersed in deuterated water for 24 h at room temperature. The SANS result was collected and analyzed using the same two-layer model used for the *d*-toluene case. Compared to the *d*-toluene sample, the samples immersed in deuterated water did not result in significant increases in SANS intensities. This result was not surprising because the thin films were macroscopically hydrophobic, that is, a drop of distilled water placed on the sample surface displayed a large contact angle. Quantitative analysis of the SANS data reveals that $(3.10\pm0.05)\%$ of the pore volume inside the film were filled by water. The quantity can be transferred into water uptake in percent mass of the sample through the relation $\Phi P\rho_{H_2O}/\rho_{\text{eff}}$, where the density of water is taken as 1 g/cm^3. The calculated water uptake at room temperature for 24 h was $(3.00\pm0.05)\%$ by mass.

F. Coefficient of thermal expansion

SXR data is an excellent technique to measure the out-of-plane coefficient of thermal expansion of thin films because the thickness of a film is easily determined from the spacing of the interference fringes. The porous film in this study was placed in a specially designed vacuum chamber and the film thickness was measured at different temperatures. The SXR measurements were conducted in vacuum in order to minimize thermal degradation or oxidation of the films. Before each measurement, the sample was held at each temperature for at least 1 h. The dependence of the film thickness with temperature determines the film CTE in a straightforward way. In the SXR data in Fig. 3, many oscillations appear between the two critical angles. These oscillations are a manifestation of optical coupling, i.e., at certain incident angles the thin porous film acts as a x-ray waveguide. The incident beam travels within the film with little intensity escaping from the film, resulting in minima in the reflected intensity. At angles greater than the θ_c of silicon, the oscillations in the SXR data are due to the interference of radiation reflected from the air/film and film/silicon interfaces. However, in the low Q_z region or region close to the θ_c of silicon, the simple relation between film thickness and the periodicity of the interference fringes is not strictly true due to multiple scattering. The film thickness is best determined from the spacing or the periodicity of the fringes in the high Q_z region. In this work, the high Q_z regime was defined as the Q_z range where the reflectivity fell below 10^{-2}. In this Q_z regime, multiple scattering constitutes less than 1% of the reflected intensity. The Fourier transform of the high Q_z data is given in Fig. 5 and the film thickness is obtained from the peak position multiplied by 2π. The film thickness results at various temperatures ranging from 25 to 175 °C is given in Fig. 6. The coefficient of thermal expan-

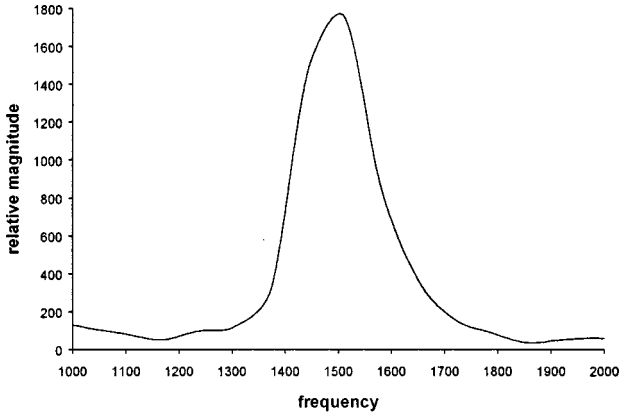

FIG. 5. Fourier transform of an x-ray reflectivity curve for data in Fig. 3 greater than $Q_z=0.035$ Å^{-1}, that is, in the periodic constructive/destructive interference fringe region. The abscissa gives the frequency in the transform while the ordinate gives the magnitude of the coefficient, or strength of the period. By multiplying the period value at the peak by 2π the film thickness is recovered.

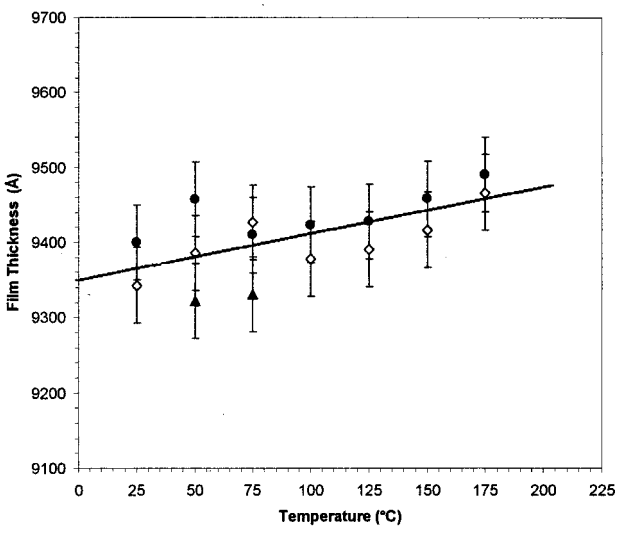

FIG. 6. Film thickness, taken from the position of the Fourier transform peak, vs temperature measured under vacuum. Two runs of the same sample are shown. The solid line is a linear regression fit to both runs. The slope of the line gives the coefficient of thermal expansion.

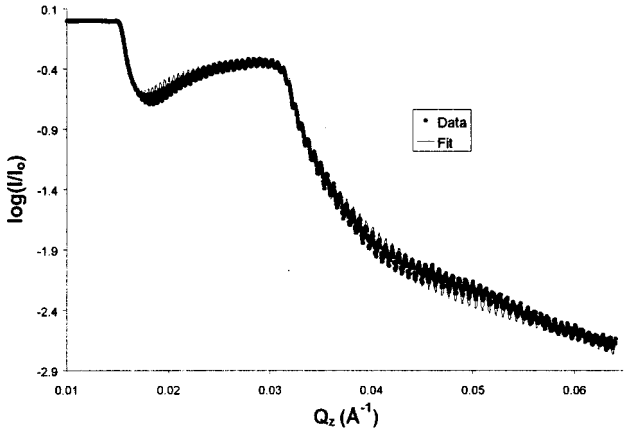

FIG. 7. Model fit to a x-ray reflectivity curve like the one shown in Fig. 3. Instead of taking the Fourier transform to determine the film thickness, a full fit of the curve gives an electron-density depth profile for the film, shown in Fig. 8.

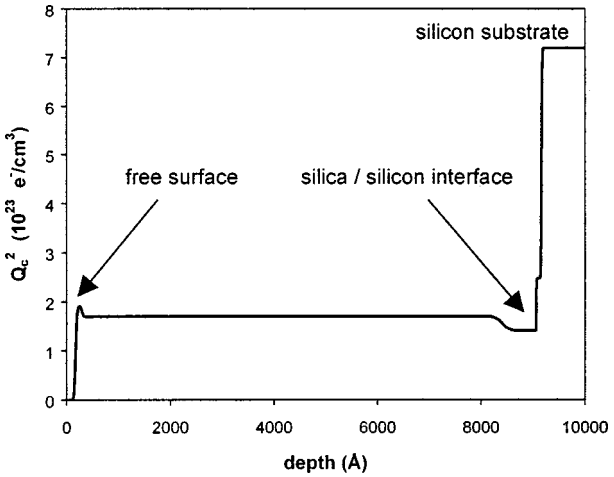

FIG. 8. Electron-density depth profile for the film shown in Fig. 7. At the extreme left is the free surface. In the free surface region, a surface ''skin'' about 5 ± 1 nm thick with an electron density slightly higher than the bulk of the film is seen. A similar layer is located at the silica/silicon interface. The plateau at the far right is the electron density of the silicon substrate.

sion (CTE), as calculated from the slope of the best fit line to the data, is $(60\pm20)\times10^{-6}/°C$. This uncertainty is due largely to the 10 nm uncertainty in the measurement of film thickness. The measurement of thicker films or of samples with a higher CTE would decrease the uncertainty of the CTE value itself.

G. Electron-density depth profile

In addition to film thickness and average film density, the SXR results can be analyzed in more detail to obtain the electron density depth profile of thin films. Information such as the location of the hydrocarbons as a function of depth within a film can be elucidated. The theoretical basis of the deconvolution of the SXR data is well established[15] and will not be repeated here. In brief, it involves the modeling of the electron density of the film normal to the surface as a series of variable-length slabs of uniform electron density. The reflectivity is calculated at each interface between all adjacent slabs. This hypothetical electron-density profile is then adjusted until the calculated reflectivity agrees well with the data. The best fit of the SXR result is given in Fig. 7 and the resultant electron-density depth profile is given in Fig. 8. This fit involves three layers (surface layer, middle layer, and interface layer) and each layer has three variables (thickness, electron density, and roughness). The silicon substrate is assigned infinite thickness, given the known electron density of silicon and a surface roughness of 2.5 nm. The surface of the porous silica thin film was found to have a roughness of 5.5 nm.

Like other scattering methods, the detailed depth profiles deduced from this analysis of SXR are not necessarily unique due to the loss of phase information. Despite this limitation, detailed analysis of SXR is valuable in many cases. For example, if the starting material profile is known, then SXR can be used to follow the time evolution of the original profile. An example pertinent to the present case is the depth distribution of hydrocarbons. If one assumes that the hydrocarbons are added after the porous film is formed and are located primarily near the free surface, the electron density of the free surface region will be higher than that near the film/substrate interface. Once a model depth profile is selected, it can be transformed into one and only one SXR profile. The validity of the model can be determined by comparing the calculated SXR and the observed one. In this way, SXR is a powerful tool to invalidate certain model depth profiles. For the current sample, the SXR result was found to be inconsistent with a model having a nonuniform density profile. The electron density profile of this sample, as shown in Fig. 8, is uniform throughout the film thickness except at the first few hundred Angstroms at both the free surface and the film/substrate interface. In light of the high content of both carbon and hydrogen, the minor density enhancements near the interfaces are not likely due to large scale segregation of hydrocarbons near the interfaces. This nonuniform density profile can be directly inferred from the data. Careful examination of Fig. 3 will show a long wavelength oscillation in the reflectivity at $Q_z=0.05\,Å^{-1}$ manifest by a slight increase in the reflectivity in this region. This feature is indicative of a layer several tens of nanometers thick in the film. Modeling the data allowed as to determine the specific nature of this layer as shown in Fig. 8.

IV. CONCLUSION

A methodology has been presented to measure the structural properties of porous silica thin film on the order of one micrometer thick and supported on silicon substrates. The method was demonstrated using AlliedSignal Nanoglass™ K2.2-A10B. High-resolution specular x-ray reflectivity provides precise measurement of film thickness and the out-of-plane coefficient of thermal expansion. In combination with composition measurements from high-energy ion scattering techniques, the average mass density can also be determined. Small angle neutron scattering, in combination with SXR and composition measurement provides the film porosity, pore connectivity, average pore size, and moisture uptake.

Modeling of the specular x-ray reflectivity data showed that there was a nonuniform electron density depth profile to the film normal to the surface.

ACKNOWLEDGMENTS

The authors would like to thank Russ Composto and Howard Wang of the University of Pennsylvania for performing the high-energy ion scattering experiments.

[1] G. K. Rao, *Multilevel Interconnect Technology* (McGraw-Hill, New York, 1993).
[2] C. Jin, J. D. Luttmer, D. M. Smith, and T. A. Ramos, MRS Bull. **22**(10), 39 (1997).
[3] L. W. Hrubesh, L. E. Keene, and V. R. Latorre, J. Mater. Res. **8**, 1736 (1993).
[4] M. Grasserbauer and H. W. Werner, *Analysis of Microelectronic Materials and Devices* (Wiley, New York, 1991).
[5] M. P. Petkov, M. H. Weber, K. G. Lynn, K. P. Rodbell, and S. A. Cohen, Appl. Phys. Lett. **74**, 2146 (1999).
[6] D. W. Gidley, W. E. Frieze, T. L. Dull, A. F. Yee, E. T. Ryan, and H. M. Ho, Phys. Rev. B **60**, R5157 (1999).
[7] M. P. Petkov, M. H. Weber, K. G. Lynn, K. P. Rodbell, and S. A. Cohen, J. Appl. Phys. **86**, 3104 (1999).
[8] J. Lekner, *Theory of Reflection* (Nijhoff, Dordrecht, 1987).
[9] S. Dietrich and A. Haase, Phys. Rep. **260**, 1 (1995).
[10] E. Chason and T. M. Mayer, Crit. Rev. Solid State Mater. Sci. **22**, 1 (1997).
[11] J. S. Higgins and H. C. Benoit, *Polymers and Neutron Scattering* (Oxford University Press, Oxford, 1994).
[12] Certain commercial materials and equipment are identified in this article in order to specify adequately the experimental procedure. In no case does such identification imply recommendation or endorsement by the National Institute of Standards and Technology, nor does it imply that the items identified are necessarily the best available for the purpose.
[13] A. T. Ramos, K. Roderick, A. Maskara, and D. Smith, Mater. Res. Soc. Symp. Proc. **443**, 91 (1997).
[14] B. C. Jin, S. List, S. Yamanaka, W. W. Lee, K. Taylor, W. Y. Hsu, L. Olsen, J. Luttmer, and R. Havemann, Mater. Res. Soc. Symp. Proc. **443**, 99 (1997).
[15] L. G. Parratt, Phys. Rev. **95**, 359 (1954).
[16] D. L. Ho, R. M. Briber, R. L. Jones, S. K. Kumar, and T. P. Russell, Macromolecules **31**, 9247 (1998).
[17] J. R. Tesmer and M. Nastasi, *Handbook of Modern Ion Beam Materials Analysis* (Materials Research Society, Pittsburgh, 1995).
[18] Q. Pan, G. B. Gonzales, R. J. Composto, W. E. Wallace, B. Arkles, L. K. Figge, and D. H. Berry, Thin Solid Films **345**, 244 (1999).
[19] P. Debye, H. R. Anderson, and H. Brumberger, J. Appl. Phys. **28**, 679 (1957).